Research Article Vol. 9, No. 10 | 1 Oct 2018 | BIOMEDICAL OPTICS EXPRESS 4979

Biomedical Optics EXPRESS

Upconversion raster scanning microscope for long-wavelength infrared imaging of breast cancer microcalcifications

YU-PEI TSENG,[1,*] PASCALINE BOUZY,[2] CHRISTIAN PEDERSEN,[1] NICK STONE,[2] AND PETER TIDEMAND-LICHTENBERG[1]

[1]*DTU Fotonik, Technical University of Denmark, Roskilde, 4000, Denmark*
[2]*School of Physics and Astronomy, University of Exeter, EX4 4QL, UK*
**yupts@fotonik.dtu.dk*

Abstract: Long-wavelength identification of microcalcifications in breast cancer tissue is demonstrated using a novel upconversion raster scanning microscope. The system consists of quantum cascade lasers (QCL) for illumination and an upconversion system for efficient, high-speed detection using a silicon detector. Absorbance spectra and images of regions of ductal carcinoma *in situ* (DCIS) from the breast have been acquired using both upconversion and Fourier-transform infrared (FTIR) systems. The spectral images are compared and good agreement is found between the upconversion and the FTIR systems.

© 2018 Optical Society of America under the terms of the OSA Open Access Publishing Agreement

1. Introduction

Breast cancer is the second most common cause of cancer death among women after lung cancer in the United States in 2018 [1]. To improve the prognosis for these patients, early and accurate diagnosis is necessary. Microcalcifications, which are abnormal deposits of calcium in the mammary gland, are a potential early marker for breast cancer [2]. They are classified according to their spatial distribution in the breast as well as their biochemical composition. In fact, two types of calcifications are observed in the breast: type I consisting of calcium oxalate mainly found in benign lesions and type II composed of calcium hydroxyapatite (Hap) involved in proliferative lesions and invasive cancer. Hap crystals $Ca_{10}(PO_4)_6(OH)_2$ often include substituted ions of carbonate (CO_3^{2-}), replacing either hydroxyl (OH^-) or phosphate (PO_4^{3-}) ions. The current method to detect these calcifications is based on X-ray mammography. But, unfortunately, this technique cannot discriminate between microcalcifications from benign and malignant lesions [2]. In contrast to mammography, vibrational spectroscopic imaging techniques can reveal the structural and molecular information from biological samples allowing for label-free characterization and diagnosis of human tissue [3]. Moreover, different studies suggest that vibrational spectroscopy could be used to discriminate the degree of the pathology in breast cancer based on their carbonate level [4].

The combination of microscopy and mid-infrared or Raman spectroscopy have progressed over the past decades and have become sensitive tools providing chemical information as well as structural details without exogenous staining of the samples [4]. Vibrational spectroscopic imaging can provide label free imaging or mapping of tissue sections to provide a spatial distribution of molecular compositions of cells and tissues, without recourse to stains. When mid-IR absorption spectra [5] or Raman inelastic scattering spectra are measured [6], at each microscopic pixel in the image, an exquisite data set can be acquired and interrogated for subtle changes associated with diseases. Raman and IR hyperspectral imaging are complimentary approaches and have been demonstrated to be able to discriminate numerous diseases based on spectral imaging of molecular changes associated with early and late diseases in various organs [7–10].

#339838 https://doi.org/10.1364/BOE.9.004979
Journal © 2018 Received 16 Jul 2018; revised 7 Sep 2018; accepted 11 Sep 2018; published 24 Sep 2018

Biomedical Optics EXPRESS

Raman spectroscopy was first demonstrated by Haka *et al.* for analysis of chemical composition of microcalcifications in the different lesions of the breast [11]. Raman spectroscopic imaging can provide complimentary vibrational molecular spectral information on tissue samples, with less sample preparation needed than IR. However, Raman is a slower method, due to the low scattering cross-section of biomolecules. In order to increase Raman signal, coherent Raman scattering (CRS) techniques have been developed [12]. It has been demonstrated that the coherent anti-Stokes Raman scattering (CARS) and stimulated Raman scattering (SRS), can provide cellular and chemical compositions from tissues, such as from calcified cartilage [13]. CRS techniques are able to provide fast label-free imaging acquisition. Raman and CRS spectroscopy have many advantages such as high speed, high resolution and no water contribution, but auto-fluorescence from the biological sample is the most important challenge. Further translation of these technologies is expected to deliver numerous tools for use on *ex vivo* fluids/cells/tissues for point of care analysis of pathology or *in vivo* clinical applications.

Fourier-Transform Infrared (FTIR) imaging is reasonably rapid (tens of minutes per spectral image) and is recognized as a highly effective and reliable method of providing spectral analysis of biological tissue samples [14]. However, FTIR is currently too slow for real-time imaging for the delivery of rapid hyperspectral pathology. In recent years, discrete frequency IR microscopes with tunable mid-IR laser sources, such as quantum cascade lasers, optical parametric oscillators or filtered supercontinuum light sources, enabling label-free classification of cancerous tissue have been demonstrated [15–20]. By tuning to a molecular absorbance wavelength of interest, real-time molecular imaging can be utilized for immediate unstained tissue analysis. Furthermore, for advanced spectral predication of disease, the Bhargava group has shown that using a confocal Agilent microscope with a QCL source coupled to a Mercury Cadmium Telluride (MCT) detector it was possible to screen automatically breast tissue biopsies (1 mm diameter) in ~1 hour, in High Definition [21].

To date all the above IR imaging techniques have relied upon detectors sensitive to mid-IR photons, i.e. Mercury Cadmium Telluride Focal Plane Array (MCT-FPA) or microbolometer, for long-wavelength infrared (LWIR) detection. However, these detectors have a signal-to-noise ratio several orders of magnitude lower than that of silicon detectors. This is mainly due to the unavoidable dark noise originating from the finite temperature of the detector. Cooling is therefore required to optimize the performance of traditional LWIR detectors. Another issue is the response time of most direct LWIR detectors being much slower than their silicon counterpart, resulting in either low signal-to-noise ratio or long acquisition time for direct LWIR detection [22].

Frequency upconversion is an alternative approach to direct detection of infrared radiation [23–25]. Converting long-wavelength infrared emission into the visible/near infrared range via nonlinear frequency conversion allows for the use of silicon detectors. Moreover, silicon detectors are low noise, fast, sensitive, and cost efficient compared to their mid-infrared counterparts. It has been demonstrated, that it is possible to detect phosphate and carbonate bands in the breast cancer microcalcifications using upconversion detection [26]. There, a silicon power meter was used to acquire the upconverted signals. Due to the limited response time of the detector, the X-Y translation stage moved to each spatial position and then waited for the detector to complete the measurement before moving to the next position. Thus, the acquisition time was approx. 20 minutes per image (the area of 1 x 1 mm^2, 20 µm step size).

In this study, we demonstrate an upconversion raster scanning microscope that allows for the characterization of the histology and chemical composition of breast cancer microcalcifications in the LWIR spectral regime. Acquisition times per wavelength of approx. 25 seconds are demonstrated for a scanned area of 1 x 1 mm^2. The histological structure and molecular information of *ex vivo* breast cancer microcalcifications is analyzed using the upconversion raster scanning microscopy system, showing nice agreement with a Micro-FTIR system.

Biomedical Optics EXPRESS

2. Materials and methods

2.1 Breast cancer sample

The *ex vivo* breast cancer biopsy with microcalcifications, obtained with ethical approval from Gloucestershire Royal Hospitals NHS Foundation Trust, was from a patient who had undergone a biopsy for mammographically suspicious breast lesions and it was selected from the histopathological report. The biopsy was embedded in paraffin and two 3 µm-thick adjacent sections were cut from the biopsy sample and analyzed. One section without staining was mounted onto a 0.5 mm-thick Barium fluoride (BaF_2) disc and analyzed using Micro-FTIR and the upconversion microscopy systems. The tissue section was required to be thin to enable sufficient IR light to penetrate the highly absorbing mineralized tissue. The other section with Hematoxylin and Eosin (H&E) staining was used for histological analysis as the gold standard reference.

2.2 Instrumentation – micro-FTIR system

FTIR imaging of the unstained breast cancer biopsy section was performed with an Agilent 620 FTIR microscope, equipped with a 15x Cassegrain objective and a 128 x 128 pixel liquid nitrogen-cooled MCT-FPA detector, and a globar source. This was coupled with an Agilent 670 FTIR spectrometer. Infrared spectra ranging from 3900 to 800 cm^{-1} were recorded with a spectral resolution of 4 cm^{-1} and a pixel size of 5.5 µm. Each spectrum was obtained by averaging 64 scans and ratioed with a background spectrum averaging 256 scans. The FTIR spectra were collected using Agilent ResolutionPro software.

2.3 Instrumentation – upconversion microscopy system

The unstained breast biopsy section, containing microcalcifications, was also analyzed using a home-built upconversion raster scanning microscope. The setup is illustrated in Fig. 1(a). A quantum cascade laser (Mini-QCL 100, BLOCK engineering) was used as a widely tunable, narrow linewidth, LWIR source tunable from 9.43 to 12 µm, delivering 50 ns pulses with a temporal separation of 1 µs. The LWIR beam was coupled to a scanning microscope allowing for mechanically stable raster scanning of the biopsy sample. The sample was placed between two ZnSe lenses, mounted on Z-axis translation mounts ($f_1 = f_2 = 20$ mm) giving a LWIR beam waist (radius) of approx. 28 µm in the sample plane (measured using knife edge scanning with the translation stage). Two lenses ($f_3 = 50$ mm and $f_4 = 150$ mm) were used to focus the transmitted LWIR and the near infrared (NIR) mixing beams, respectively, into a nonlinear crystal via a beam combiner. In the nonlinear crystal, the LWIR beam is mixed with the mixing beam for sum frequency generation. An 8 W diode laser was used to pump a $Nd:YVO_4$ laser generating the 1064 nm single-pass mixing field, giving a maximum output power of 3W in continuous-wave operation. The sum frequency generation (SFG) was realized in a 5 x 5 x 10 mm^3 $AgGaS_2$ crystal. The $AgGaS_2$ crystal was cut at $\theta = 43.3°$ ($\phi = 0$) for collinear type II phase-matching ($e_{LWIR} + o_{NIR} \rightarrow e_{Up}$). The $AgGaS_2$ crystal was mounted on a piezo controlled rotation stage (ECR3030, Attocube) for angle tuned birefringent phase-matching, converting the LWIR signal to the 950 to 980 nm range. For further details see ref [25]. Three short-pass filters (FESH1000, Thorlabs) and a long-pass filter (FELH900, Thorlabs) were used in line before the upconverted signals were detected with a silicon detector (PDA 100A, Thorlabs).

Biomedical Optics EXPRESS

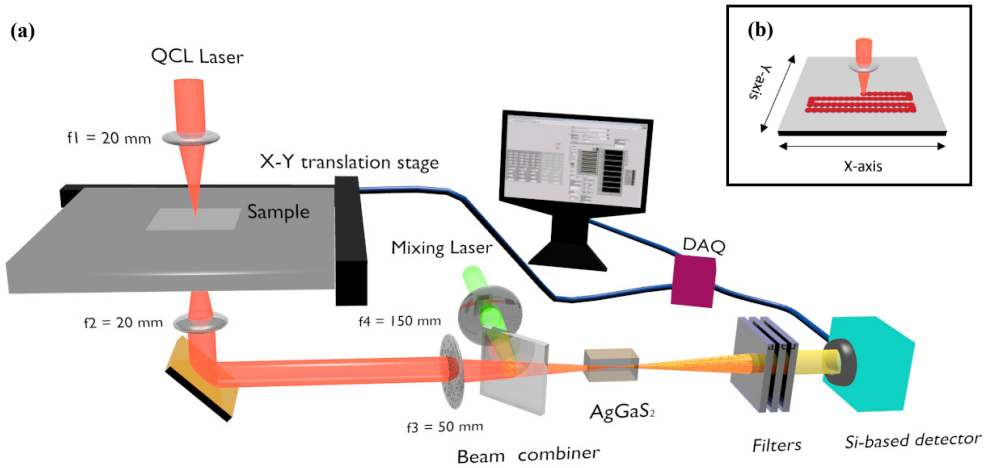

Fig. 1. (a). Schematic layout of experimental setup for upconversion raster scanning microscope. (b) Raster scanning scheme.

The X-Y translation stage scans in two dimensions using raster scanning, as shown in Fig. 1(b). The stage moves in the X-direction (fast axis) with a constant velocity of 5 mm/s and in the Y-axis with a step size of 10 µm (between the strips in X-axis). The X-Y translation stage has angular encoders on the axis spindles providing two quadrature electric signals to allow for tracking of the position. The X-Y positions and the analogue signal from the silicon detector were processed by the Data Acquisition module (DAQ National Instruments NI-6251). The sampling rate of the DAQ module is set to 100 kHz taking samples simultaneously from the Analog to Digital Converter (ADC) and the position decoders. The upconverted signals from the silicon detector was low-pass filtered with a 1 kHz analog passive filter, giving a response, which preserves the signal representing the features in the target, but rejects unwanted high-frequency components (essentially working as an anti-aliasing filter). Because the sampling rate is 500 times the bandwidth of the signal of interest, there is a wide frequency range for this analogue filter to operate in and it can be made as a simple first-order passive filter. To remove all signals outside the band of interest the digital data stream was subsequently digitally filtered by a Finite Impulse Response (FIR) low-pass filter (Filter Express VI, LabVIEW) with the low-pass frequency at 200 Hz (at 0.1 dB). This filter has an impulse response with a full-width half maximum of approx. 0.6 ms, which corresponds to a spatial translation of 3 µm at the scanning speed of 5 mm/s. As this width is much smaller than the illumination beam diameter of 56 µm, the filter only slightly deteriorates the combined spatial resolution. The filtered signals were then binned according to the corresponding position (X,Y) and accommodated into an image array with a pixel size of 10 µm x 10 µm. Finally, the image is resampled into an expanded array with a pixel size of 1.8 µm x 1.8 µm, cropping the field of view to remove regions with non-constant scanning speed at the end of each X-scan (where the scanning direction is changed).

3. Results and discussion

3.1 Illumination area of the sample

The LWIR illumination beam was measured in the plane of the biological sample, using the knife-edge method. Knifes were placed on the X-Y translation stage, and scanned across the LWIR beam in both the X- and Y-directions. The transmitted LWIR signal was upconverted

Biomedical Optics EXPRESS

and detected with the silicon detector. The measured beam size in the object plane using this approach was found to be Gaussian with an approx. beam diameter of 56 µm.

3.2 Air Force 1951 resolution target

The performance of the upconversion microscopy is demonstrated imaging a USAF 1951 resolution target. The resolution target was placed on the X-Y translation stage for raster scanning and illuminated by the LWIR beam at 970 cm^{-1}. The transmitted light was mixed with the 1064 nm laser for sum frequency generation, giving an upconversion signals at 964 nm. The upconverted signal was detected with the silicon detector. Figure 2(a) and (b) show upconversion images of the resolution target group 2 and 3, respectively. The intensity profiles across the horizontal set of bars (red/blue dashed lines) are illustrated in Fig. 2(c) and (d), respectively. The target features are well resolved corresponding to a resolution higher than 35 µm (Group 3, element 6). The decreasing intensity in Fig. 2(d) for the finer structures reflects the narrow aperture compared to the larger illumination beam, however, the modulation between the lines clearly shows that the lines are spatially resolved.

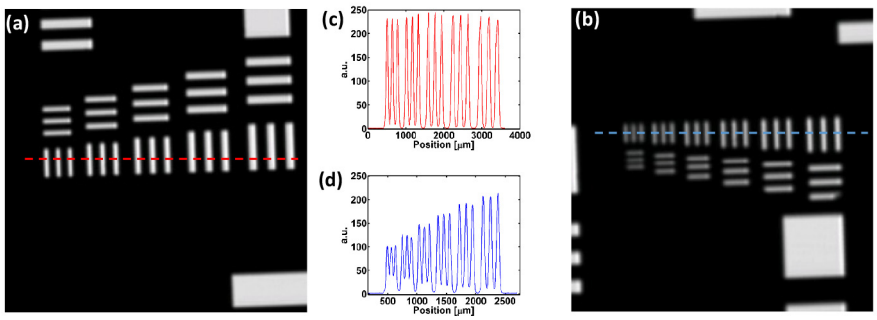

Fig. 2. USAF 1951 optical resolution target (a) group 2, element 2-6 (b) group 3, element 1-6 imaged with the upconversion raster scanning microscope in transmission. Images displayed were obtained at 970 cm^{-1} (10.31 µm) corresponding to the upconverted signal at 964 nm. Intensity profiles across the horizontal set of bars (red/blue dashed lines) were plotted in (c) and (d) respectively.

3.3 Microcalcifications from an ex vivo sample of breast DCIS

The study presented here aims to develop a diagnostic tool, to analyze breast cancer tissue biopsies in the 1060 to 830 cm^{-1} spectral range, retrieving spectral information related to the phosphate and carbonate bands. In this region, these bands are not overlaid by paraffin signal. Discrete wavelength tuning is a time efficient approach to acquire the spectral signatures of the tissue sample under investigation.

Figure 3(a) shows a histological section of *DCIS* with H&E staining and transmission microscope examination of the tissue. The adjacent unstained section was evaluated using micro-FTIR imaging, see Fig. 3(b), and the upconversion raster scanning microscopy systems, see Fig. 3(c). The FTIR and upconverted images were measured at the phosphate peak at 1020 cm^{-1}. The LWIR signal transmitted through the sample was upconverted from 1020 cm^{-1} into the near infrared (958.8 nm) and detected using the silicon detector. The area (approx. 0.5 mm^2), corresponding to microcalcification area in the biopsy sample, was marked with the black squares in Fig. 3. The acquisition time of the FTIR image, with area of 0.5 mm^2 as a single image tile of FTIR averaged by 64 scans in the spectral range of 3900-800 cm^{-1} at the interval of 4 cm^{-1}, was approx. 5 minutes, and a monochromatic image with the same area can be measured in 30 seconds using the upconversion system. The actual acquisition time using the upconversion system mainly depends on the number of wavelengths needed to identify the microcalcifications and the desired image size. The acquisition time is currently limited by the scan speed of the X-Y translation stage, but higher

Biomedical Optics EXPRESS

scan speed will reduce the signal-to-noise ratio as a result of reduced integration time of the individual spatially resolvable element.

Comparing the FTIR image and upconversion image in Fig. 3(b) and (c), the absorbance measurements generally show good agreement. However, in the center of the calcified regions, the absorbance is significantly higher in the upconversion image compared to the FTIR image, this is believed to be a result of the coherent illumination used in the upconversion system [27].

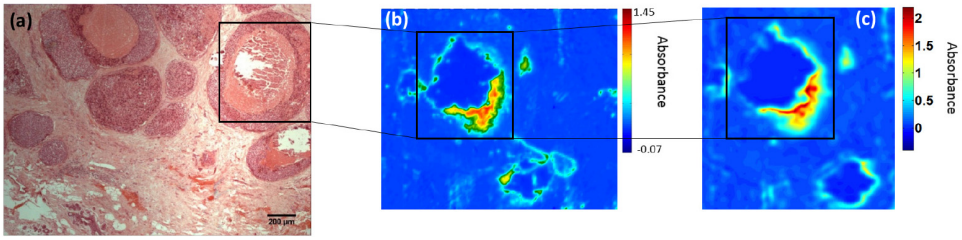

Fig. 3. Histological section of *DCIS* breast cancer microcalcifications with H&E staining imaged with the transmission microscope. The area marked with the black squares is approx.0.5 mm^2. (b) FTIR absorbance image with the size of approx.1.4 mm x 1.7 mm referring to phosphate peak at 1020 cm^{-1} (c) Upconversion absorbance image with the size of approx.1.3 mm x 1.2 mm obtained at 1020 cm^{-1} corresponding to the upconverted signal at 958.8 nm.

Only few discrete wavelengths are required to identify the microcalcifications for the phosphate and carbonate bands at 1020 cm^{-1} and 875 cm^{-1}. In order to map out the spectral features of the microcalcifications and compare the spectra, multispectral imaging was performed with the upconversion system and compared to spectra obtained with the Micro-FTIR system. Figure 4(a) shows the multispectral images obtained with upconverted at 1040, 1032, 1020, 1005, 970, 962, 950, 910, 881, 875, 860, and 850 cm^{-1}. The wavelength of interest was set for the QCL with an illumination bandwidth of ~1 cm^{-1} and the nonlinear crystal was rotated for optimal conversion efficiency for each wavelength [25]. Reference measurements on an empty area of the BaF_2 sample mount were performed at each wavelength for calculation of the sample absorbance. Figure 4(b) shows absorbance spectra obtained using the Micro-FTIR (solid lines) and upconversion system (dots) for a region of comedo *DCIS* (containing a microcalcification), and Fig. 4(c) shows the corresponding absorbance spectra measured in an area of non-cancerous connective tissue (not containing calcifications). The FTIR system becomes noisy in the LWIR regime (900 to 800 cm^{-1}), resulting in spectral artifacts. The upconverted absorbance was retrieved from the series of images illustrated in Fig. 4(a) and extracted from the area where the phosphate band is highly absorbing (pink arrow) and from surrounding tissue (orange arrow). A significant decrease in the signal (increased absorbance) is seen at the phosphate absorption band in the microcalcification area (pink arrow) compared to the surrounding. The carbonate peak is also seen at the signal around 875 cm^{-1}. The upconverted spectrum shows a good agreement with FTIR spectrum. Generally, upconversion detection gives a superior SNR at low signal levels (high absorbance's due to the very low dark noise in the Si detector) [28,29]. This is highly pertinent to the highly absorbing breast calcifications, and may allow for the use of thicker samples.

Biomedical Optics EXPRESS

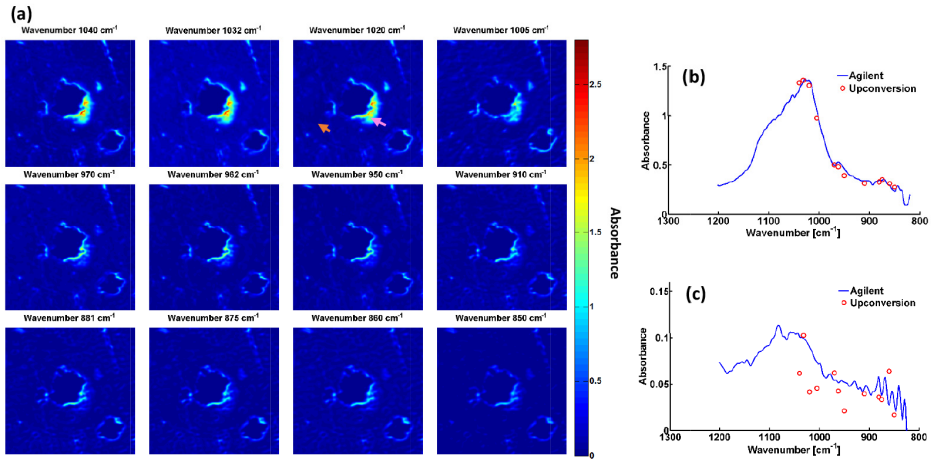

Fig. 4. (a) Multispectral upconversion images of the *DCIS* breast microcalcifications obtained at 1040, 1032, 1020, 1005, 970, 962, 950, 910, 881, 875, 860, and 850 cm^{-1} corresponding to the upconverted signals in the range of 958 to 976 nm. Spectra measured using Micro-FTIR (Agilent) and upconversion systems from (b) microcalcification (pink arrow) and (c) surrounding tissue (orange arrow) in breast sample. It is noticeable that absorbance obtained in microcalcification (b) and surrounding tissue (c) are in a different scale.

4. Conclusion

We demonstrate that breast cancer tissues can be analyzed using the upconversion raster scanning microscopy system without the use of exogenous staining. The use of upconversion can enable fast image acquisition compared to FTIR microscopic imaging, through the use silicon detectors, potentially improving speed and the signal-to noise ratio, even at low cost and without the need for cryogenic cooling. The presented result shows excellent agreement between upconversion raster scanning microscopy and Micro-FTIR imaging, in terms of spatial distribution and spectral features of breast microcalcifications. Discrete wavelength turning can reduce the acquisition time, depending on the number of wavelengths needed for diagnoses. This new approach has the potential to measure fresh tissue samples, without the need for exogenous staining, and with much improved speed over Micro-FTIR imaging.

Funding

European Union Horizon 2020 research innovation programme (642661).

Acknowledgments

The authors gratefully acknowledge Mr. Henning Engelbrecht Larsen for the support of LabVIEW programing and electronics.

Disclosures

The authors declare that there are no conflicts of interest related to this article.

References

1. C. E. DeSantis, J. Ma, A. Goding Sauer, L. A. Newman, and A. Jemal, "Breast Cancer Statistics, 2017, racial disparity in mortality by state," CA Cancer J. Clin. **67**(6), 439–448 (2017).
2. R. Baker, K. D. Rogers, N. Shepherd, and N. Stone, "New relationships between breast microcalcifications and cancer," Br. J. Cancer **103**(7), 1034–1039 (2010).
3. C. Kendall, M. Isabelle, F. Bazant-Hegemark, J. Hutchings, L. Orr, J. Babrah, R. Baker, and N. Stone, "Vibrational spectroscopy: A clinical tool for cancer diagnostics," Analyst (Lond.) **134**(6), 1029–1045 (2009).

Biomedical Optics EXPRESS

4. M. Sattlecker, R. Baker, N. Stone, and C. Bessant, "Support vector machine ensembles for breast cancer type prediction from mid-FTIR micro-calcification spectra," Chemom. Intell. Lab. Syst. **107**(2), 363–370 (2011).
5. M. Hermes, R. B. Morrish, L. Huot, L. Meng, S. Junaid, J. Tomko, G. R. Lloyd, W. T. Masselink, P. Tidemand-Lichtenberg, C. Pedersen, F. Palombo, and N. Stone, "Mid-IR hyperspectral imaging for label-free histopathology and cytology," J. Opt. **20**, 2 (2018).
6. H. J. Butler, L. Ashton, B. Bird, G. Cinque, K. Curtis, J. Dorney, K. Esmonde-White, N. J. Fullwood, B. Gardner, P. L. Martin-Hirsch, M. J. Walsh, M. R. McAinsh, N. Stone, and F. L. Martin, "Using Raman spectroscopy to characterize biological materials," Nat. Protoc. **11**(4), 664–687 (2016).
7. G. Shetty, C. Kendall, N. Shepherd, N. Stone, and H. Barr, "Raman spectroscopy: elucidation of biochemical changes in carcinogenesis of oesophagus," Br. J. Cancer **94**(10), 1460–1464 (2006).
8. N. Stone, C. Kendall, J. Smith, P. Crow, and H. Barr, "Raman spectroscopy for identification of epithelial cancers," Faraday Discuss. **126**, 141–157, discussion 169–183 (2004).
9. N. Stone, M. C. Hart Prieto, P. Crow, J. Uff, and A. W. Ritchie, "The use of Raman spectroscopy to provide an estimation of the gross biochemistry associated with urological pathologies," Anal. Bioanal. Chem. **387**(5), 1657–1668 (2007).
10. J. Nallala, G. R. Lloyd, N. Shepherd, and N. Stone, "High-resolution FTIR imaging of colon tissues for elucidation of individual cellular and histopathological features," Analyst (Lond.) **141**(2), 630–639 (2016).
11. A. S. Haka, K. E. Shafer-Peltier, M. Fitzmaurice, J. Crowe, R. R. Dasari, and M. S. Feld, "Identifying microcalcifications in benign and malignant breast lesions by probing differences in their chemical composition using Raman spectroscopy," Cancer Res. **62**(18), 5375–5380 (2002).
12. M. J. Baker, H. J. Byrne, J. Chalmers, P. Gardner, R. Goodacre, A. Henderson, S. G. Kazarian, F. L. Martin, J. Moger, N. Stone, and J. Sulé-Suso, "Clinical applications of infrared and Raman spectroscopy: state of play and future challenges," Analyst (Lond.) **143**(8), 1735–1757 (2018).
13. J. Mansfield, J. Moger, E. Green, C. Moger, and C. P. Winlove, "Chemically specific imaging and in-situ chemical analysis of articular cartilage with stimulated Raman scattering," J. Biophotonics **6**(10), 803–814 (2013).
14. K. Das, C. Kendall, M. Isabelle, C. Fowler, J. Christie-Brown, and N. Stone, "FTIR of touch imprint cytology: a novel tissue diagnostic technique," J. Photochem. Photobiol. B **92**(3), 160–164 (2008).
15. C. Kuepper, A. Kallenbach-Thieltges, H. Juette, A. Tannapfel, F. Großerueschkamp, and K. Gerwert, "Quantum cascade laser-based infrared microscopy for label-free and automated cancer classification in tissue sections," Sci. Rep. **8**(1), 7717 (2018).
16. M. R. Kole, R. K. Reddy, M. V. Schulmerich, M. K. Gelber, and R. Bhargava, "Discrete Frequency Infrared Microspectroscopy and Imaging with a Tunable Quantum Cascade Laser," Anal. Chem. **84**(23), 10366–10372 (2012).
17. A. Ogunleke, V. Bobroff, H. H. Chen, J. Rowlette, M. Delugin, B. Recur, Y. Hwu, and C. Petibois, "Fourier-transform vs. quantum-cascade-laser infrared microscopes for histo-pathology: From lab to hospital?" TrAC - Trends Analyt. Chem. **89**, 190–196 (2017).
18. N. Kröger, A. Egl, M. Engel, N. Gretz, K. Haase, I. Herpich, B. Kränzlin, S. Neudecker, A. Pucci, A. Schönhals, J. Vogt, and W. Petrich, "Quantum cascade laser-based hyperspectral imaging of biological tissue," J. Biomed. Opt. **19**(11), 111607 (2014).
19. K. Yeh, S. Kenkel, J. N. Liu, and R. Bhargava, "Fast infrared chemical imaging with a quantum cascade laser," Anal. Chem. **87**(1), 485–493 (2015).
20. C. R. Petersen, N. Prtljaga, M. Farries, J. Ward, B. Napier, G. R. Lloyd, J. Nallala, N. Stone, and O. Bang, "Mid-infrared multispectral tissue imaging using a chalcogenide fiber supercontinuum source," Opt. Lett. **43**(5), 999–1002 (2018).
21. S. Mittal, K. Yeh, L. S. Leslie, S. Kenkel, A. Kajdacsy-Balla, and R. Bhargava, "Simultaneous cancer and tumor microenvironment subtyping using confocal infrared microscopy for all-digital molecular histopathology," Proc. Natl. Acad. Sci. U.S.A. **115**(25), E5651–E5660 (2018).
22. A. Rogalski, *Infrared Detectors* (CRC Press, 2015).
23. P. Tidemand-Lichtenberg, J. S. Dam, H. V. Andersen, L. Høgstedt, and C. Pedersen, "Mid-infrared upconversion spectroscopy," J. Opt. Soc. Am. B **33**(11), D28 (2016).
24. J. S. Dam, P. Tidemand-Lichtenberg, and C. Pedersen, "Room-temperature mid-infrared single-photon spectral imaging," Nat. Photonics **6**(11), 788–793 (2012).
25. Y.-P. Tseng, C. Pedersen, and P. Tidemand-Lichtenberg, "Upconversion detection of long-wave infrared radiation from a quantum cascade laser," Opt. Mater. Express **8**(5), 1313–1321 (2018).
26. Y. P. Tseng, P. Bouzy, N. Stone, C. Pedersen, and P. Tidemand-Lichtenberg, "Long wavelength identification of microcalcifications in breast cancer tissue using a quantum cascade laser and upconversion detection," Proc. SPIE **10490**, 1049001 (2018).
27. S. Ran, S. Berisha, R. Mankar, W. C. Shih, and D. Mayerich, "Mitigating fringing in discrete frequency infrared imaging using time-delayed integration," Biomed. Opt. Express **9**(2), 832–843 (2018).
28. L. Høgstedt, J. S. Dam, A.-L. Sahlberg, Z. Li, M. Aldén, C. Pedersen, and P. Tidemand-Lichtenberg, "Low-noise mid-IR upconversion detector for improved IR-degenerate four-wave mixing gas sensing," Opt. Lett. **39**(18), 5321–5324 (2014).

Biomedical Optics EXPRESS

29. L. Meng, A. Fix, M. Wirth, L. Høgstedt, P. Tidemand-Lichtenberg, C. Pedersen, and P. J. Rodrigo, "Upconversion detector for range-resolved DIAL measurement of atmospheric CH_4," Opt. Express **26**(4), 3850–3860 (2018).